# EXPERIMENTAL STUDY ON INFLUENCES OF KINEMATIC VISCOSITY ON OCCURENCES OF CAVITATION DUE TO SUB-SURFACE VORTEX

T. Ezure<sup>1</sup>, N. Kimura<sup>1</sup>, J. Kobayashi<sup>1</sup> and H. Kamide<sup>1</sup> Japan Atomic Energy Agency, Oarai-machi, Ibaraki-ken, Japan

#### **Abstract**

In order to clarify the influence of kinematic viscosity ( $\nu$ ) on the occurrence of vortex cavitation, a water experiment was carried out in a cylindrical tank with a suction pipe. The occurrences of vortex cavitation were measured under several fluid temperature conditions between 10°C and 80°C ( $\nu$ : 1.3x10<sup>-6</sup> to 3.7x10<sup>-6</sup>m<sup>2</sup>/s). The velocity fields around vortex were also measured by Particle Image Velocimetry. The influence of  $\nu$  was observed under relatively high  $\nu$  conditions. However, that influence diminished with the increase of  $\nu$  or suction velocity. And also, normalized circulation  $\Gamma^*$  was found as an index to estimate such influences of  $\nu$  or suction velocity on the vortex cavitation.

#### Introduction

In the design of Japan Sodium Cooled Fast Reactor (JSFR) [1], the cooling systems are planned to be reduced to two loops, while former sodium cooled fast reactors such as "Monju" have three loops. The mean coolant velocity at the intakes of hot leg (H/L) pipes reaches up to 9.2m/s in the JSFR design. Thus, the cavitation due to sub-surface vortex (vortex cavitation) initiated from the high coolant velocity can occur between the H/L intake and reactor vessel (R/V) wall [2]. Figure 1 shows the overview of JSFR R/V (left side one) and an example of vortex cavitation at the H/L intake observed in a water model test [2]. In the right side snapshot, three cavitating vortex tubes (cavity) were seen as the white line. The restriction of this type of cavitation is a key issue for the structural integrity of the reactor.

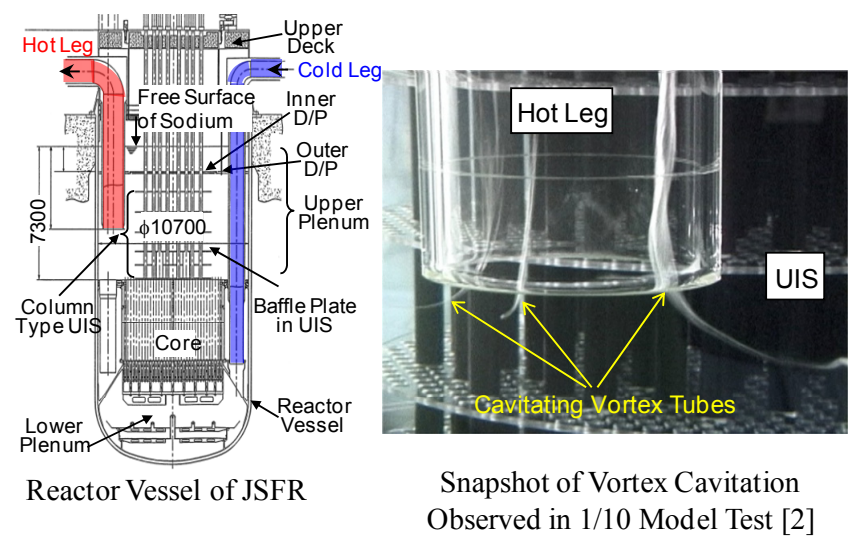


Figure 1 Reactor vessel of JSFR and example of vortex cavitation at a hot leg inlet (water experiment)

Vortex cavitation has been well-researched in the turbo machinery field for the pump sumps. As for the evaluation of occurrence, standards for scale model tests are published from American National Standard Institute [3] or Turbomachinery Society of Japan [4]. Those standards require the same working fluid and geometry as the real plant in the model test. If these guidelines were applied directly to JSFR, a sodium experiment in a similar geometry to JSFR would be required. However, that kind of mock up experiment has difficulties in experimental methods how to detect vortex cavitation in the complicated geometry. Thus, it is required to develop an evaluation method which can predict the occurrence of vortex cavitation from the water model experiments based on the knowledge of fundamental water and sodium experiments. In other words, the final goal of this study is to establish an evaluation method without the sodium mockup experiments. Therefore, it is crucial to obtain the fundamental knowledge about the differences on vortex cavitation between sodium and water

There are several experiments on occurrence of cavitation concerning the difference between sodium and water [5][6]. Those experiments were mainly performed in orifices, throats or such kind of geometry, i.e., pressure dropping devices in plants. Those results suggest that an experiment in water can give conservative results about the occurrence of cavitation than that in sodium. However, there are few works about the occurrence of vortex cavitation. The vortex cavitation occurs due to the pressure decrease at the vortex center. This pressure decrease will depend on structure of the vortex, e.g., characteristic radius. Especially, the influence of kinematic viscosity ( $\nu$ ), which is 1/3 smaller in sodium, must to be clarified in terms of the pressure decrease at vortex center.

In order to obtain the fundamental knowledge on vortex cavitation, a water experiment [7] was performed in a simple cylindrical tank geometry to grasp the characteristics of cavitating vortex. That geometry has one suction pipe at the center of the tank and a single vortex cavitation is generated at the intake of suction pipe. In the present study, the occurrences of vortex cavitation were measured under several fluid temperature conditions between 10°C and 80°C ( $\nu$ :  $1.3 \times 10^{-6}$  to  $3.7 \times 10^{-6}$  m<sup>2</sup>/s) to clarify the influences of fluid viscosity. The velocity fields around vortex were also measured by Particle Image Velocimetry(PIV) [8] to quantify the influence of  $\nu$  on the strength of circulation and the velocity distributions of vortex structure.

## 1. Vortex cavitation and cavitation factor

# 1.1 Evaluation using cavitation factor

Cavitation is a kind of phase change process due to the local pressure drop. Therefore, cavitation factor,  $\sigma$  is ordinary used as an index to evaluate the intensity of cavitating flow as follows;

$$\sigma = \frac{P_s - P_v}{\frac{1}{2} \rho V^{*2}} \tag{1}$$

 $P_s$  is the system pressure at a local point.  $P_v$  is the vapor pressure.  $\rho$  is the fluid density.  $V^*$  is a characteristic velocity. For instance in the 1/10 R/V model test [2],  $V^*$  was defined as the mean velocity in H/L. This index of  $\sigma$  is defined as the ratio of static pressure divided by dynamic pressure. A fluid is thought to cavitate at  $\sigma \le 1$  based on the Bernoulli's principle in an ideal situation. Thus, it is also expected that vortex cavitation will occur at the same strength under the constant  $\sigma$  condition (pressure balance assumption). However, in the actual situation,  $\sigma$  at the onset of cavitation depends

on various factors, such as geometry, working fluid or others. Especially, in case of vortex cavitation, the influence of  $\nu$  is also anticipated as mentioned in the next section 1.2.

# 1.2 Influence of fluid viscosity on the pressure drop at the vortex center

Based on the Burgers model [9], the local pressure  $drop(\Delta P_l)$  in a stretch vortex is thought to depend on  $\nu$ . In the Burgers model,  $\Delta P_l$  at a vortex center owing to the centrifugal force of swirl flow can be expressed as follows;

$$\Delta P_l = \ln 2 \cdot \rho \left( \frac{\Gamma_{\infty}}{2\pi r_1} \right)^2 \tag{2}$$

where,  $\Gamma_{\infty}$  is circulation at infinite distance.  $r_{I}$  is the specific radius of vortex as follows;

$$r_1 = 2\sqrt{\frac{\nu}{\alpha}} \tag{3}$$

where,  $\alpha$  is the axial velocity gradient. From Eqs. (2) and (3),  $\Delta P_l$  becomes larger with the decrease of  $\nu$ . Therefore, it is considered that vortex cavitation occurs easily in the small  $\nu$  fluid in case that  $\Gamma$  and  $\alpha$  varied proportionally to  $V^*$ . As the results, pressure balance assumption would not be proper to evaluate vortex cavitation occurrence, if the Burgers model can be applied directly to the evaluation of vortex cavitation.

In the present study, influences of  $\nu$  on the occurrences of vortex cavitation are evaluated from the point whether the pressure balance assumption is applicable to the evaluation of vortex cavitation under the different  $\nu$  conditions.

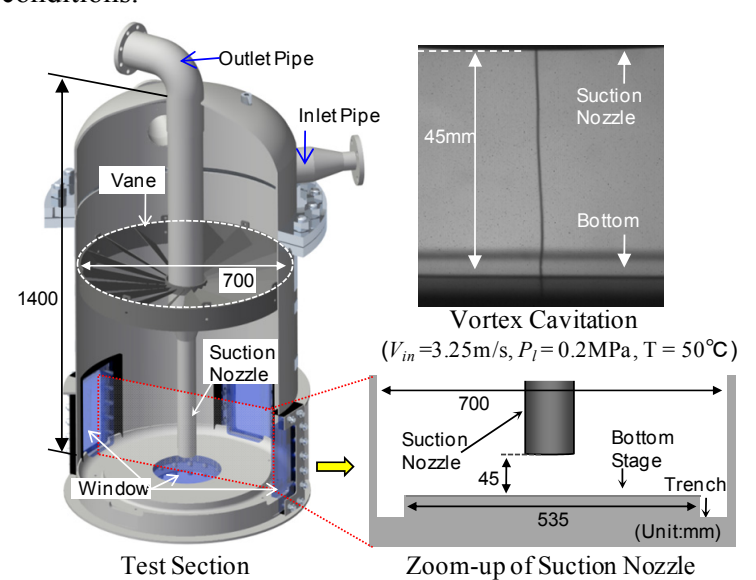


Figure 2 Overview of test section and example of vortex cavitaion

# 2. Experiments

## 2.1 Experimental apparatus for vortex cavitation

A water experiment was performed in cylindrical tank geometry. Figure 2 shows the overview of test section and an example of visualized image of vortex cavitaion. The test section(left picture) is a

vertical cylindrical tank(height:1400mm, diameter:φ700mm). Water flows in from the upper region of the tank and flows out through a suction nozzle. The bottom of tank has φ535mm flat stage at the center to have a vortex on its surface (see the right side zoom up). There is a circular trench of 30mm depth between the center stage and side wall to dump the disturbance from the side wall. The suction nozzle was inserted vertically at the center of tank. This suction nozzle is a straight pipe of 55mm inner diameter having the sharp edge. The end of suction nozzle inlet was set at 45mm height from the bottom. There are four transparent side windows and one bottom window to visualize the inside of test section as shown in Figure 2.

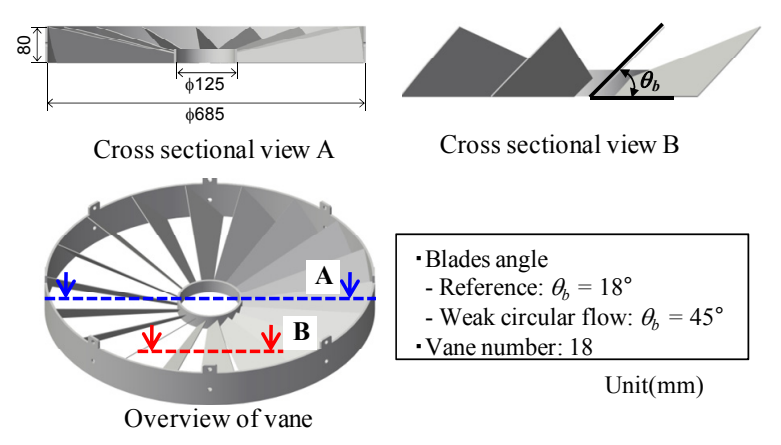


Figure 3 Overview of propellers generating the swirl flow

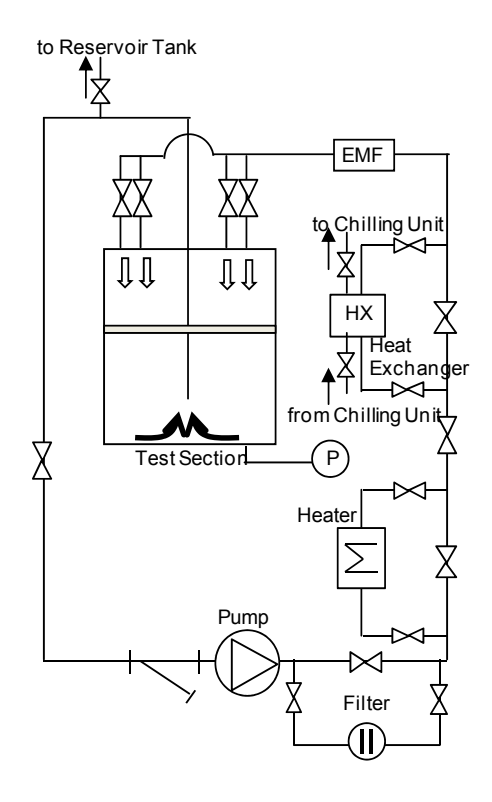


Figure 4 Schematic diagram of test loop

Inclined blades (vane) to generate the swirl flow were also set at 690 mm above the bottom window (see, white broken circle in Figure 2). Figure 3 shows the schematic of the vanes. The 18 flat vanes

having a certain attack angle are assembled with circumferentially equal spans to circulate the fluid. This slow and swirl flow in the tank of 700mm diameter is converged into the nozzle of 55mm diameter. As the results, a vortex is developed by this strong convergence and suction flow. Two attack angles of blades ( $\theta_b = 18^\circ$  and  $\theta_b = 45^\circ$ ) from the horizontal plane were selected to change the swirl flow strength. Here,  $\theta_b = 18^\circ$  is reference geometry and the swirl flow thorough the 45° vane can be roughly three times weaker than that in 18° vane.

Figure 4 shows the schematic diagram of the test loop. Water is circulated by a mechanical pump though the test loop. Water temperature is adjusted by an electric heater and a chilling unit. The test loop has only one free surface in the reservoir tank to pressurize the system. The flow path between the reservoir tank and main loop was regulated by a valve to reduce influences of the dissolved oxygen. Related to the geometry, several experimental parameters are defined, here. The suction velocity  $V_{in}$  is defined as the mean velocity at suction nozzle.  $P_l$  is defined as the static pressure at the bottom of test section. Therefore,  $\sigma$  in Eq. (1) was defined using  $V_{in}$  and  $P_l$  as follows;

$$\sigma = \frac{P_l - P_v}{\frac{1}{2} \rho V_{in}^2} \tag{4}$$

Water temperature T is monitored at the inlet of test section using a K-type thermocouple.

#### 2.2 Measurement condition

# 2.2.1 Visualization measurement of vortex cavitation

The occurrences of vortex cavitation were measured by a combination of visualization and image analysis. Figure 5 shows the experimental setup to visualize the vortex cavitation. Visualized images of vortex cavitation were captured through a side window of the tank by a digital camera. The back lighting method was also employed to reduce the halation at the surface of cavity. A metal halide lump was used as a light source. A semi-transparent sheet was inserted between the test section and the lump as a light diffuser to get a uniform lighting. Surface shapes of vortex cavitation were captured by a digital CMOS camera with 64k pixels(252x240) of imaging elements. The imaging area was set as nearly 45mm(H) x 42mm(W) region between the bottom of the test section and the inlet of suction nozzle. Therefore, the spatial resolution of image was nearly 0.18mm/pixel. Continuous 18000 frames of image were captured with 33.3ms of sampling interval (30Hz sampling), i.e., 10 minutes measurement in each experimental case.

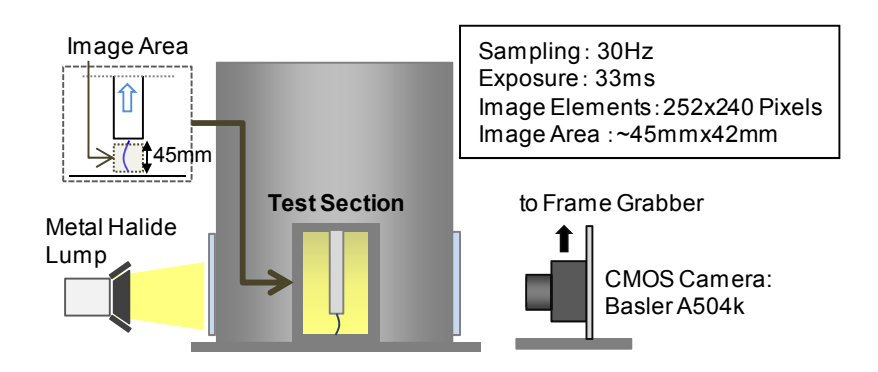


Figure 5 Measurement setup for the visualization of vortex cavitation

# 2.2.2 Measurement of horizontal velocity

The horizontal velocity distributions were obtained by PIV. Measurements were performed at 10mm above the bottom of test section. The size of measurement area was approximately, 140mm×140mm. The velocity field was obtained by the cross-correlation method with sub-pixel accuracy [10]. The typical spatial resolution of each velocity vector was 0.3mm (22x22 pixels of reference window). The sampling interval of velocity field was 62.5Hz. The total sampling time was nearly 16s (1024 times sampling at 62.5Hz).

# 2.4 Experimental condition

Table 1 shows the parameter range of visualization experiments. Here,  $\theta_b$ , T and  $P_l$  were treated as primary experimental parameters.  $V_{in}$  was treated as subsidiary parameter of  $P_l$ , since  $V_{in}$  was a parameter which contributes to the local pressure balance as same as  $P_l$ . As mentioned in section 2.1,  $\theta_b$  was set at 18°( Reference geometry ) or 45°( Weak swirl flow geometry ). In order to evaluate the influence of fluid viscosity, the water temperature T was varied within the range from 10°C to 80°C. Therefore, the kinematic viscosity of water, v, was varied from 1.3 x 10<sup>-6</sup> m<sup>2</sup>/s to 3.7 x 10<sup>-7</sup> m<sup>2</sup>/s and  $P_v$  was also varied from 1.2 to 47.5kPa, according to the increase of T. This increase of  $P_v$ , which influence the sub-cool, is considered in  $\sigma$  as shown by Ep. (4).  $P_l$  was changed within the range from 0.1 MPa(absolute pressure) and 0.6MPa. Dissolved oxygen was controlled up to 0.05mg/l. Table 2 shows the representative temperature conditions that are discussed in detail in the latter sections. The PIV measurements were performed especially in Case B (T=30°C) and Case D (T=80°C).

Table 1 Parameter range of vifuzalization experiment

$\theta_b(\deg)$	T(°C)	$v(\text{m}^2/\text{s})$	$V_{in}(\text{m/s})$	$P_l$ (MPa)
18,45	10 - 80	$1.3 \times 10^{-6} - 3.7 \times 10^{-7}$	0 - 11	0.1* - 0.65**

<sup>\*</sup>no-pressurizing condition, \*\* at T > 40°C, 0.60 MPa was maximum

Table 2 Representative temparature conditions

	$T(^{\circ}\mathbb{C})$	$v(\text{m}^2/\text{s})$	$P_{\nu}$ (kPa)	$\theta_b(\deg)$
Case A	10	$1.3 \times 10^{-6}$	1.2	
Case B	30	$8.0 \times 10^{-7}$	4.2	18
Case C	50	$5.5 \times 10^{-7}$	12.3	10
Case D	80	$3.7x10^{-7}$	47.5	
Case E	30	$8.0 \times 10^{-7}$	4.2	45
Case F	80	$3.7x10^{-7}$	47.5	43

#### 3. Results and discussions

# 3.1 Visualized image of vortex cavitation and quantitative detection procedure

The left side picture in Figure 6 shows the typical image of vortex cavitation observed in case of  $T = 20^{\circ}\text{C}$ ,  $V_{in} = 5.25\text{m/s}$  and  $P_{l} = 0.2\text{MPa}$ . Vortex cavitation is seen as a column shaped shadow between the bottom and the suction nozzle inlet. The occurrence of vortex cavitation was judged by image

analysis. Detection area of cavity is 24mm x 34mm of square area shown by yellow line. Here, the noisy area due to the structure such as the suction nozzle or bottom was eliminated.

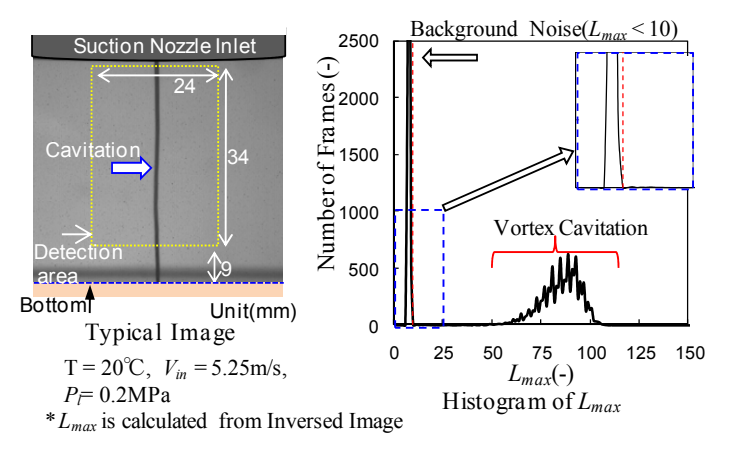


Figure 6 Image analysis procedure

The right side graph in Figure 6 shows the histogram of the maximum luminance difference  $L_{max}$ . The vertical broken line shows  $L_{max} = 10$ .  $L_{max}$  was defined as the maximum value of luminance difference within the detection area at the every instantaneous image. The luminance difference  $L_{def}$  was calculated from the difference of the luminance value between every instantaneous image and representative image. The representative image was selected from no cavitating image.

It was observed that there are two peaks in  $L_{max}$  distribution within  $L_{max} > 10$  and  $L_{max} < 10$ , respectively. One peak in the relatively high luminosity range (between  $L_{max}$ =75 amd  $L_{max}$ =100) shows the frames when the vortex cavitation existed. Another peak in the low luminosity range( $L_{max}$  < 10) shows the background noise. Threfore, vortex cavitation occurrence was judged by setting a threshold value between these two peaks.

# 3.2 Experimental Result in Reference( $\theta_b$ =18°) Geometry

# 3.2.1 Variation of yield fraction of vortex cavitation

In several cases, vortex cavitation can occur intermittently. Here, an index, the yield fraction(Y.F.), was defined to evaluate the anticipation of vortex cavitation occurrences quantitatively, although for such intermittent vortex, as follows;

$$Y.F. = \frac{N_{cavi}}{N_{all}}$$
 (5)

 $N_{cavi}$  is the number of frames where the cavitation is observed.  $N_{all}$  is the total frame number ( $N_{all} = 18000$ ).

Figure 7 shows relation between  $\sigma$  and Y.F. with parameter of  $P_l$  in the reference geometry ( $\theta_b$ =18°). The left side graph, Figure 7 (1) shows the result in large  $\nu$  case, Case B(T= 30°C). Here, the horizontal axis shows  $\sigma$ . The vertical axis shows Y.F. Solid symbols are experimental results and gray lines are eye guides of Y.F. variation. Y.F. increased with the decrease of  $\sigma$  within the same  $P_l$  condition. This means the vortex cavitation occurrences increased with the increase of  $V_{in}$  from Eq. (4). From the comparison among the different  $P_l$  results, the rising edges (from zero to 0.1) shifted to the right side with the increase of  $P_l$  (see the eye guides). If the pressure balance assumption in Eq.

(1) is true, the rising curves should be identical among the cases of  $P_l = 0.2$ , 0.4 and 0.6MPa. This means that vortex cavitation had dependence on  $V_{in}$  under the large  $\nu$  condition compared to the prediction of pressure balance assumption. In other words, vortex cavitation occurred easier under relatively high  $P_l$  conditions.

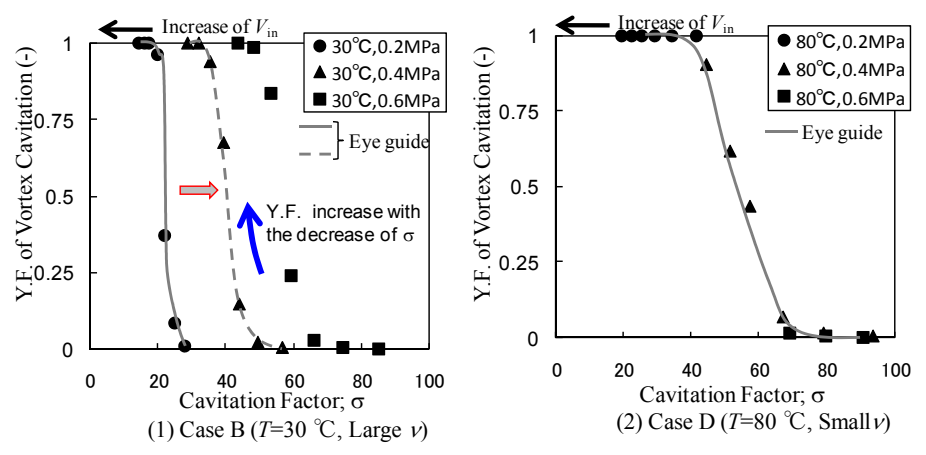


Figure 7 Relation between  $\sigma$  and Y.F. with parameter  $P_1$ 

The right side graph, Figure 7 (2) shows the result in small  $\nu$  case, Case D(T= 80°C). In this case, Y.F. data were plotted nearly on an identical curve as shown by eye guide. The strength of vortex cavitation was expressed by the nearly constant  $\sigma$  conditions independent on the  $P_l$ . This means the pressure valance assumption was valid under the small  $\nu$  condition.

# 3.2.2 <u>Influence of the kinematic viscosity</u>

Figure 8 shows the comparison of Y.F. between different temperature conditions(= $\nu$ ) with respect to the influence of  $\nu$ . The horizontal and vertical axes are plotted as same as Figure 7. Y.F. was compared in the two different ranges of  $\nu$ , large  $\nu$  range (Cases A [T= 10°C] and B [T= 30°C]) and small  $\nu$  range (Cases C [T= 50°C] and D [T= 80°C]). The variation rates of  $\nu$  are nearly the same in the two ranges ( $\nu$ =30/ $\nu$ =10  $\sim$  0.62,  $\nu$ =80/ $\nu$ =50  $\sim$  0.67,).

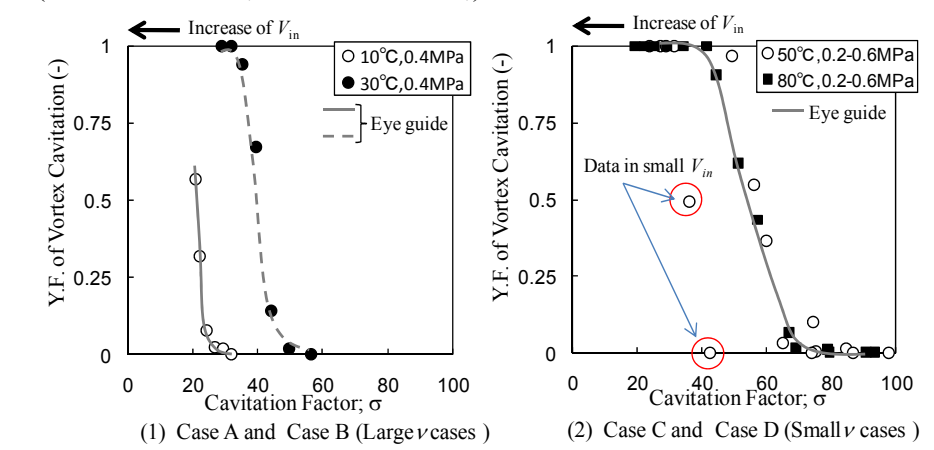


Figure 8 Comparison of Y.F. between Different Temperature Conditions

In Figure 8 (1), the rising edge (from zero to 0.1) of Y.F. in Case B ( $T=30^{\circ}$ C) shifted to the large  $\sigma$  (= right) side as compared with that in Case A( $T=10^{\circ}$ C). This means vortex cavitation occurred easily

under the smaller  $\nu$  condition of Case B. Thus, it was shown that  $\nu$  influenced the occurrence of vortex cavitation under the large  $\nu$  conditions (T= 10 - 30°C).

In Figure 8 (2), Y.F. was plotted nearly on an identical line both in Cases C and D except the two departed data obtained under relatively small  $V_{in}$  conditions in Case C(see the red circles). The influence of  $\nu$  was small as compared with the result in large  $\nu$  cases. As the result, there was not the significant influence of  $\nu$ , i.e., the pressure balance assumption was valid, at least under the small  $\nu$  conditions.

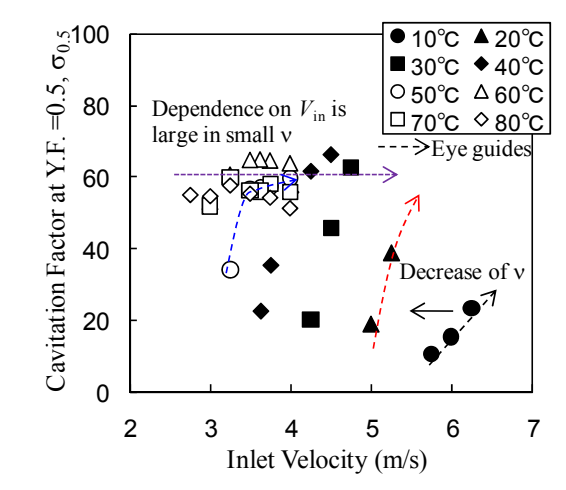


Figure 9 Comparison of circumferential velocity distribution between the different fluid temperatures (T=30, 80, Vin=4.0m/s)

From Figures 7 and 8, the influences of  $\nu$  and  $P_l(=V_{in})$  are obvious under the large  $\nu$  conditions. On the other hands, the pressure balance assumption is valid under the small  $\nu$ . In order to discuss this tendency quantitatively, a representative parameter,  $\sigma_{0.5}$  is used. The definition of  $\sigma_{0.5}$  is the cavitation factor which gives the Y.F. of 0.5. Figure 9 shows relation between  $V_{in}$  and  $\sigma_{0.5}$  with the parameter of T. The horizontal axis shows  $V_{in}$ . The vertical axis shows  $\sigma_{0.5}$ . Under relatively low T conditions, i.e., large  $\nu$  conditions,  $\sigma_{0.5}$  increased according to the increase of  $V_{in}$  as shown by the black eye guid. In these conditions,  $\sigma_{0.5}$  also increased according to the increase of T from the comparison between red and black eye guides. On the other hand,  $\sigma_{0.5}$  was nearly constant under relatively high T conditions against to the variation of  $V_{in}$  or T as shown by purple eye guide. At the intermediate temperature (see blue eye guides),  $\sigma_{0.5}$  increased at small  $V_{in}$  (< 3.5m/s), but  $\sigma_{0.5}$  became nearly constant under relatively large  $V_{in}$  (> 3.5) conditions. Thus, it was shown that the intensity of vortex cavitation became represented by  $\sigma$  (pressure balance assumption) according to the decrease of  $\nu$  or increase of  $V_{in}$ .

## 3.3 Influence of swirl flow strength

In this section, influences of swirl flow strength are discussed. Figure 10 shows relation between  $\sigma$  and Y.F. in the weak swirl flow geometry geometry ( $\theta_b$ =45°) with parameter of  $P_l$ . The left side graph, Figure 10 (1), shows the results in the large  $\nu$  case of Case E (T= 30°C). As the comparison, the results in Case B ( $\theta_b$ =18°, T= 30°C) at  $P_l$ =0.2MPa are also shown as open symbol. In Case E, the curves of Y.F. has similar tendencies to those in Case B(see, Figure 7), i.e, the intensity of vortex cavitation had dependence on  $V_{in}$  (or  $P_l$ ). However, the Y.F. curve in Case E, 0.2MPa (solid circles)

shifts to the small  $\sigma$  side (=left side) with compared to the result in Case B, 0.2MPa.  $\sigma$  at the rising edge of Y.F. curve became roughly three times smaller ( $\sigma$ ~10) than that in Case B( $\sigma$ ~30).

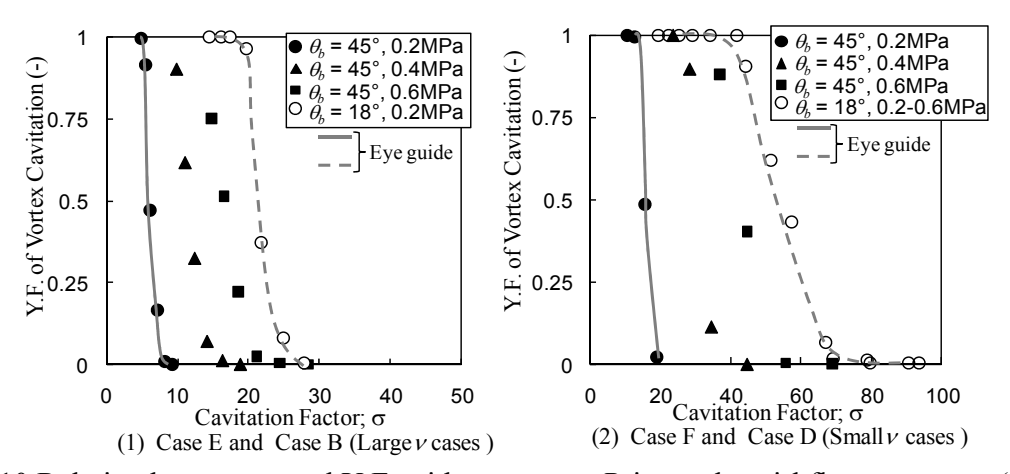


Figure 10 Relation between  $\sigma$  and Y.F. with parameter  $P_l$  in weak swirl flow geometry ( $\theta_b$ =45°)

The right side graph, Figure 10 (2) shows results in small  $\nu$  case, Case F (T= 80°C). The results in Case D at  $P_l$  =0.2-0.6MPa are also shown as open symbol. In Case F, the Y.F. did not matched on one line as Case D and the rising edge of Y.F. shifts to right side with the increase of  $P_l$ . Thus, the dependence on  $P_l$  (= $V_{in}$ ) was observed under the small  $\nu$  condition in the weak swirl flow geometry.

From these results, it was suggested that the strength of swirl flow is also the key for the  $\nu$  dependency that was observed in the reference geometry.

## 3.4 Comparison of local velocity distributions around vortex

Figure 11 shows the comparison of time averaged velocity distributions under the different  $V_{in}$  and  $\nu$  conditions. Figure 11(1), shows the time averaged velocity distributions in Case B,  $V_{in}$  =4.0, 4.5, and 5.0m/s, i.e., comparison under the different  $V_{in}$  conditions. Horizontal axis shows the horizontal position, x. Here, x and y-directions (coordinate settings) are as depicted as in the left side sketches. The center of inlet nozzle is positioned at x, y = zero. The vertical axis shows  $\overline{V_y}/V_{in}$  at y = zero. Here,  $\overline{V_y}$  is the time averaged velocity in y-direction. The vortex is nearly stable horizontally at the center of inlet nozzle (see the snapshot in Figure 6). Therefore, it is assumed that  $\overline{V_y}/V_{in}$  at y = zero can indicate the strength of circumferential flow. In this graph, the central region of vortex between x = -0.015 to 0.015m was eliminated because of the over range from the dynamic range of PIV, i.e., error of cross correlation due to the large deformation of tracer pattern between two images. Therefore, only the surrounding parts are compared here. Velocity distributions were nearly the same and independent on  $V_{in}$ . This result shows that the circulation at the surrounding part of vortex was nearly proportional to  $V_{in}$ .

Figure 11 (2) shows the time averaged velocity distributions in Cases B (T= 30°C) and D (T= 30°C), at  $V_{in}$  = 4.0m/s, i.e., comparison under different  $\nu$  conditions at the same  $V_{in}$ . The central region was eliminated also in this case as same as Figure 11(1). Velocity distributions in each case were nearly the same also in this graph. This result shows that the circulation at the surrounding part of was not affected by  $\nu$ .

From the results of Figures 11 (1) and (2), it is ensured that the swirl flow strength as the local boundary condition of vortex was determined only by  $V_{in}$ . It means that flow patterns were analogous at least in the surrounding area of vortex. Thus, it is also suggested that the variation of Y.F. shown in 3.2 was resulted from the variation of inner vortex structure near the vortex center that was not measured in this study.

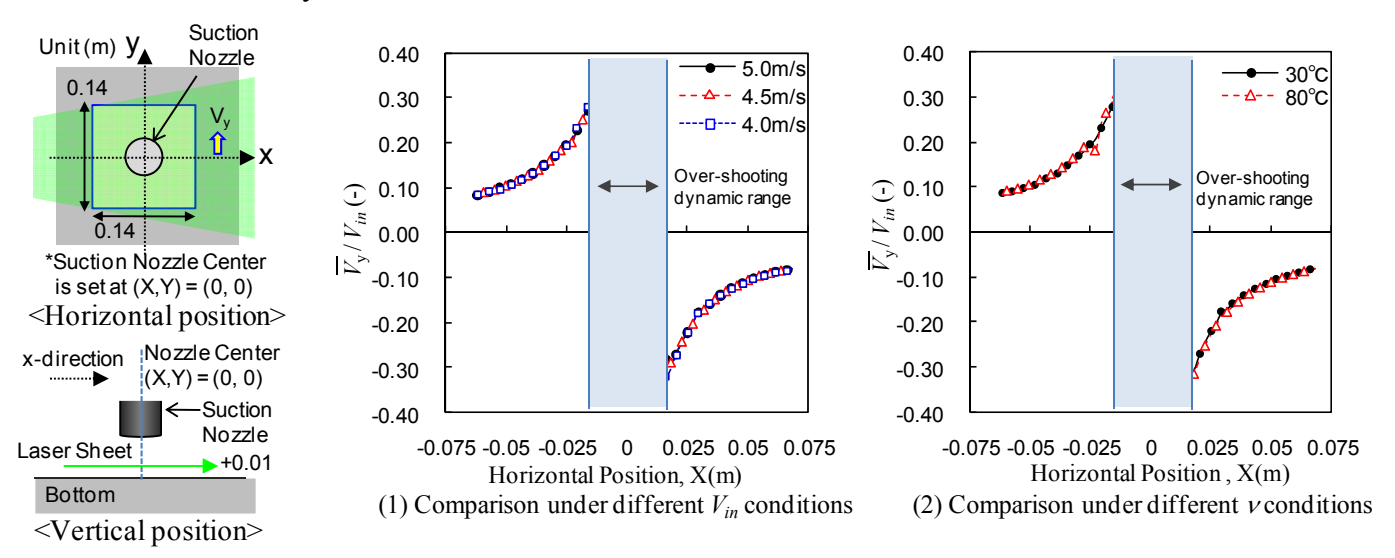


Figure 11 Comparison of time averaged velocity distributions under different  $V_{in}$  and v conditions

# 3.5 Evaluation of Vortex Cavitation Occurrence using $\Gamma^*$

From the section 3.2, it was clarified that there is some region where  $\nu$  and  $V_{in}$  must be considered, in addition to  $\sigma$ , for the evaluation of vortex cavitation occurrence. The range of that region was thought to be influenced by the strength of swirl flow from the result of section 3.3. Threfore, another parameter is proposed to express these influences.

Here, Eq. (2) is normalized under the estimation of  $\Gamma_{\infty} \sim UD$  and  $\alpha \sim U/D$ . U and D denote characteristic velocity and characteristic length, respectively.

$$\frac{\rho U^2}{\Delta P_l} \cdot \frac{UD}{v} = const \tag{6}$$

From Eq. (1),  $\rho U^2/\Delta P_l$  can be is proportional to  $1/\sigma$ . Another part of  $UD/\nu$  is the non dimensional term which represents the ratio of inertia and viscous force. Here, the numerator UD can represent the strength of swirl flow by estimating  $\Gamma_{\infty} \sim UD$ . Thus, this parameter can be the non-dimensional parameter of circulation  $\Gamma^*$  [11] as follows;

$$\frac{\sigma}{\Gamma^*} = const \tag{7}$$

Figure 12 shows occurrence map of vortex cavitaion in the relation of  $\Gamma^*$  and  $\sigma$ . Here,  $\Gamma^*$  was defined as follows;

$$\Gamma^* = \frac{V_{circ} \cdot D}{V} \tag{8}$$

where,  $V_{circ}$  is the mean circumferential velocity just under the vane.  $V_{circ}$  is thought to be proportional to  $V_{in}$  in the present experimental geometry as shown in the results of section 3.4. D is

defined as the inner diameter of suction nozzle. The horizontal axis shows  $\Gamma^*$ . The vertical axis shows  $\sigma$ . Y.F. is expressed by the color legend. The dotted line is an eye guide that was drawn at the boundary where Y.F. decreased steeply. This boundary corresponds to onset condition of the vortex cavitation. In the small  $\Gamma^*$  region ( $\Gamma^* < \sim 0.7 \times 10^3$ ),  $\sigma$  at the boundary of Y.F. increased with the increase of  $\Gamma^*$ . From the definition of Eq. (8), small  $\Gamma^*$  means the large  $\nu$  or small  $V_{circ}$ . On the other hand, the boundary of Y.F. can be expressed by nearly constant  $\sigma$  in the large  $\Gamma^*$  region ( $\Gamma^* > \sim 0.7 \times 10^4$ ). Here, large  $\Gamma^*$  means the small  $\nu$  or large  $V_{circ}$ .

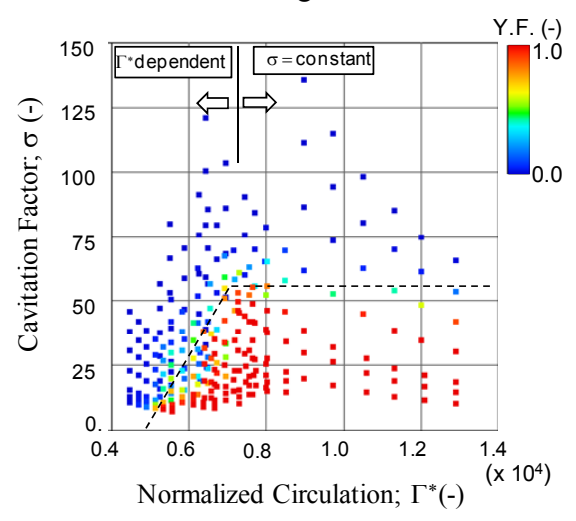


Figure 12 Occurrence map of vortex cavitaion in the relation of  $\Gamma^*$  and  $\sigma$ 

As the results, it is shown that the pressure drop at the vortex center increases according to the increase of  $\Gamma^*$  following the Burgers model shown in section 1.2. However, in large  $\Gamma^*$  region ( $\Gamma^* > \sim 0.7 \times 10^3$ ) the pressure drop hits a peak and can be expressed by a line of  $\sigma = \text{constant}$ , i.e., pressure balance assumption. The reason of this transition is not clear. However, it is supposed the contribution of kinematic viscosity becomes small in  $\sigma = \text{const}$  region and the turbulent viscosity would be a dominant viscous factor.

#### 4. Conclusions

A fundamental experiment in cylindrical water tank geometry was performed under several water temperature conditions and different two swirl flow strength geometry to clarify the influences of fluid viscosity on the occurrence of vortex cavitation. Occurrences of vortex cavitation were evaluated using the cavitation factor  $\sigma$  and the yield fraction(Y.F.). As the result, following findings were obtained.

- 1) Influence of kinematic viscosity:
  - ✓ Influence of  $\nu$  or  $V_{in}$  on vortex cavitation was observed under the large  $\nu$  conditions (T= 10 30°C in reference geometry).
  - ✓ The occurrence of vortex cavitation was expressed by the nearly constant  $\sigma$  conditions under the relatively high  $V_{in}$  or small  $\nu$  conditions (T= 50 80°C in reference geometry).
- 2) Influence of strength of swirl flow:
  - ✓ Influence of  $\nu$  or  $V_{in}$  on vortex cavitation was observed under all temperature conditions(T=50-80°C) in weak temperature geometry.
- 3) Velocity profile was independent on the  $\nu$  or  $V_{in}$  at least in the surrounding area of vortex.

4) Normalized circulation  $\Gamma^*$  was suggested as the index to evaluate the occurrence of cavitation under the different  $V_{in}$ ,  $P_l$  and  $\nu$  conditions were plotted as a map using  $\Gamma^*$ ,  $\sigma$  and Y.F..

# Acknowledgements

The authors appreciate Mr. Watanabe in MFBR Co., Ltd, Dr. Shiraishi in MHI Co., Ltd, Dr. Eguchi in CRIEPI, and Dr. Ito in JAEA for their advices on data evaluation. In addition, the authors thank to Mr. Ito in Ascend Corp. on their assistance in experiments and also Mr. Kameyama in NDD Corp. on his support in image analysis.

## 5. References

- [1] K. Aoto, et al., "Design Study and R&D Progress on Japan Sodium-Cooled Fast Reactor", Journal of Nuclear Science and Technology, Vol. 48, No. 4, 2011, pp. 463–471.
- [2] N. Kimura, et al, "Noise Reduction Techniques for the Particle Image Velocimetry -Application to an Experimental Study on Natural Convection in a Fast Reactor Core-", <u>Proceedings of 8th International Conference on Nuclear Engineering</u>, Baltimore, Maryland, USA, 2000.
- [3] American National Standard Institute "American National Standard for Pump Intake Design" ANSI/HI9.8, 1998.
- [4] Turbomachinery Society of Japan, "Standarad method for Model Testing the Performance of a Pump Sump", TSJ S 002, 2005.
- [5] A.E. Collinson, "The Onset of Cavitation in Pressure Dropping Dvices in Water and Sodium", International Working Group on Fast Reactors, Specialists Meeting on Cavitation in Sodium and Studies of Analogy with Water as Compared to Sodium (IWGFR 9), Cadarache, France, 1976, pp33-41.
- [6] J.R. Bonnin, "Thermodynamic Effect in Cavitation", Conference on Cavitation held at Herriot-Watt Univ., Edinburgh, UK, 1974, pp355-362.
- [7] T. Ezure, et al, "Influences of fluid viscosity on the occurrences of cavitation due to sub-surface vortex", <u>Proceeding of The Seventh Korea-Japan Symposium on Nuclear Thermal Hydraulics and Safety</u>, Chuncheon, Korea, 2010, November 14- 17.
- [8] Adrian, R. J., "Particle-imaging techniques for experimental fluid mechanics", Ann. Rev. Fluid Mech., Vol.23, 1991, pp.261-304
- [9] J. M. Burgers, "A mathematical model illustrating the theory of turbulence", Advances in applied mechanics edited by R. Mises, T. Karman, Academic Press ING, New York, 1948.
- [10] J. Sakakibara, et al, "Measurements of Thermally Stratified Pipe Flow Using Image Processing Techniques", Experiments in Fluids, Vol.16,1993, pp 82-96.
- [11] T. Sakai, et al. "Proposal of Design Criteria for Gas Entrainment from Vortex Dimples Based on a Computational Fluid Dynamics Method", Heat Transfer Engineering, Vol.29, 2008, pp.731-739.